The Astrophysical Journal, 850:206 (10pp), 2017 December 1 https://doi.org/10.3847/1538-4357/aa95c0
© 2017. The American Astronomical Society. All rights reserved.

Direct Observations of Different Sunspot Waves Influenced by Umbral Flashes

Aishawnnya Sharma[1,2], G. R. Gupta[2], Durgesh Tripathi[2], V. Kashyap[3], and Amit Pathak[1,4]
[1] Department of Physics, Tezpur University, Tezpur 784028, India
[2] Inter-University Centre for Astronomy and Astrophysics, Post Bag-4, Ganeshkhind, Pune 411007, India; girjesh@iucaa.in
[3] Harvard-Smithsonian Center for Astrophysics, Cambridge, MA, USA
Received 2016 August 24; revised 2017 October 9; accepted 2017 October 22; published 2017 December 4

Abstract

We report the simultaneous presence of chromospheric umbral flashes and associated umbral waves, and propagating coronal disturbances, in a sunspot and related active region. We have analyzed time–distance maps obtained using the observations from the Atmospheric Imaging Assembly on board the *Solar Dynamics Observatory*. These maps show the simultaneous occurrence of different sunspot oscillations and waves such as umbral flashes, umbral waves, and coronal waves. Analysis of the original light curves, i.e., without implementing any Fourier filtering on them, shows that the amplitudes of different sunspot waves observed at different atmospheric layers change in synchronization with the light curves obtained from the umbral flash region, thus demonstrating that these oscillations are modulated by umbral flashes. This study provides the first observational evidence of the influence of sunspot oscillations within the umbra on other sunspot waves extending up to the corona. The properties of these waves and oscillations can be utilized to study the inherent magnetic coupling among different layers of the solar atmosphere above sunspots.

Key words: Sun: chromosphere – Sun: corona – Sun: oscillations – Sun: photosphere – sunspots – waves

1. Introduction

Waves play an important role in the heating of the upper atmosphere of the Sun. Different features observed over sunspots at different atmospheric heights host a variety of waves, such as the 5-minutes photospheric oscillations, the 3-minute chromospheric oscillations, umbral flashes and waves, running penumbral waves (RPWs), and propagating coronal waves (see, e.g., reviews by Bogdan & Judge 2006; De Moortel & Nakariakov 2012; Sych 2016). Although these oscillations and waves have been studied for decades, we are still far from understanding the physics behind their origin and the possible coupling among them. It has further been suggested that sunspot waves and oscillations may play an important role in the initiation of solar flares and coronal mass ejections, as well as solar wind acceleration (see, e.g., Sych 2016). Recent studies show that sunspot waves may also play an important role in the triggering of coronal jets (Chandra et al. 2015). Jets were triggered during the growing amplitude phase of the waves; however, the cause of such an amplitude increase is still unknown.

Umbral flashes are observed as sudden strong brightenings occurring at random locations in the sunspot umbrae, with a period of around 3 minutes in chromospheric lines, and are considered the first observations of sunspot oscillations (Beckers & Tallant 1969). These are strongly nonlinear oscillations with asymmetric light curves, where the increase in the amplitude is steeper than the decrease, giving it a sawtooth shape. Such light curves are interpreted as signatures of upward-propagating magnetoacoustic shock waves (e.g., Rouppe van der Voort et al. 2003; Centeno et al. 2006). The shock wave nature of sunspot oscillations has also been recently reported in the transition region lines (Tian et al. 2014). The RPWs are outward-propagating intensity waves with a period of about 5 minutes and are observed in the chromospheric penumbrae of sunspots (Zirin & Stein 1972). These oscillations are interpreted as upward-propagating magnetoacoustic waves guided by the magnetic field and originate in the lower atmosphere (Bloomfield et al. 2007; Jess et al. 2013).

The relationships between 3-minute umbral waves and 5-minute RPWs are still not fully understood. While some studies have advocated that they are different manifestations of a common phenomenon (Christopoulou et al. 2001; Tziotziou et al. 2006; Thomas & Weiss 2008), other studies suggest an unclear relationship between them (Christopoulou et al. 2000; Kobanov & Makarchik 2004; Kobanov et al. 2006). Recently, Madsen et al. (2015) claimed that both umbral flashes and running waves originate from photospheric p-mode oscillations, where umbral flashes were preceding the running waves in both the spatial and temporal domains.

Propagating intensity disturbances along various coronal structures with periods between 3 and 20 minutes are ubiquitous in the solar corona (De Moortel 2009; De Moortel & Nakariakov 2012). The loop-like structures, which are often rooted in the umbra, show outward-propagating intensity disturbances with periods around 3 minutes, whereas those rooted in non-sunspot regions show periods around 5 minutes (e.g., De Moortel et al. 2002). Furthermore, open plume and interplume structures in the polar region also show outward-propagating intensity disturbances with periods around 10–30 minutes (e.g., Gupta et al. 2010; Krishna Prasad et al. 2011). These propagating disturbances are found to have wave-like properties and are often interpreted in terms of propagating slow magnetoacoustic waves (e.g., Gupta et al. 2012; Kiddie et al. 2012). Although these coronal wave disturbances are ubiquitous in the different structures, observational evidence of their source region is still missing.

Recently, Jess et al. (2012) found 3-minute magnetoacoustic waves in the coronal fanloops that were rooted into the photosphere at locations where large-amplitude 3-minute umbral dot oscillations were observed. Krishna Prasad et al. (2015)

[4] Current Address: Department of Physics, Banaras Hindu University, Varanasi 221005, India.

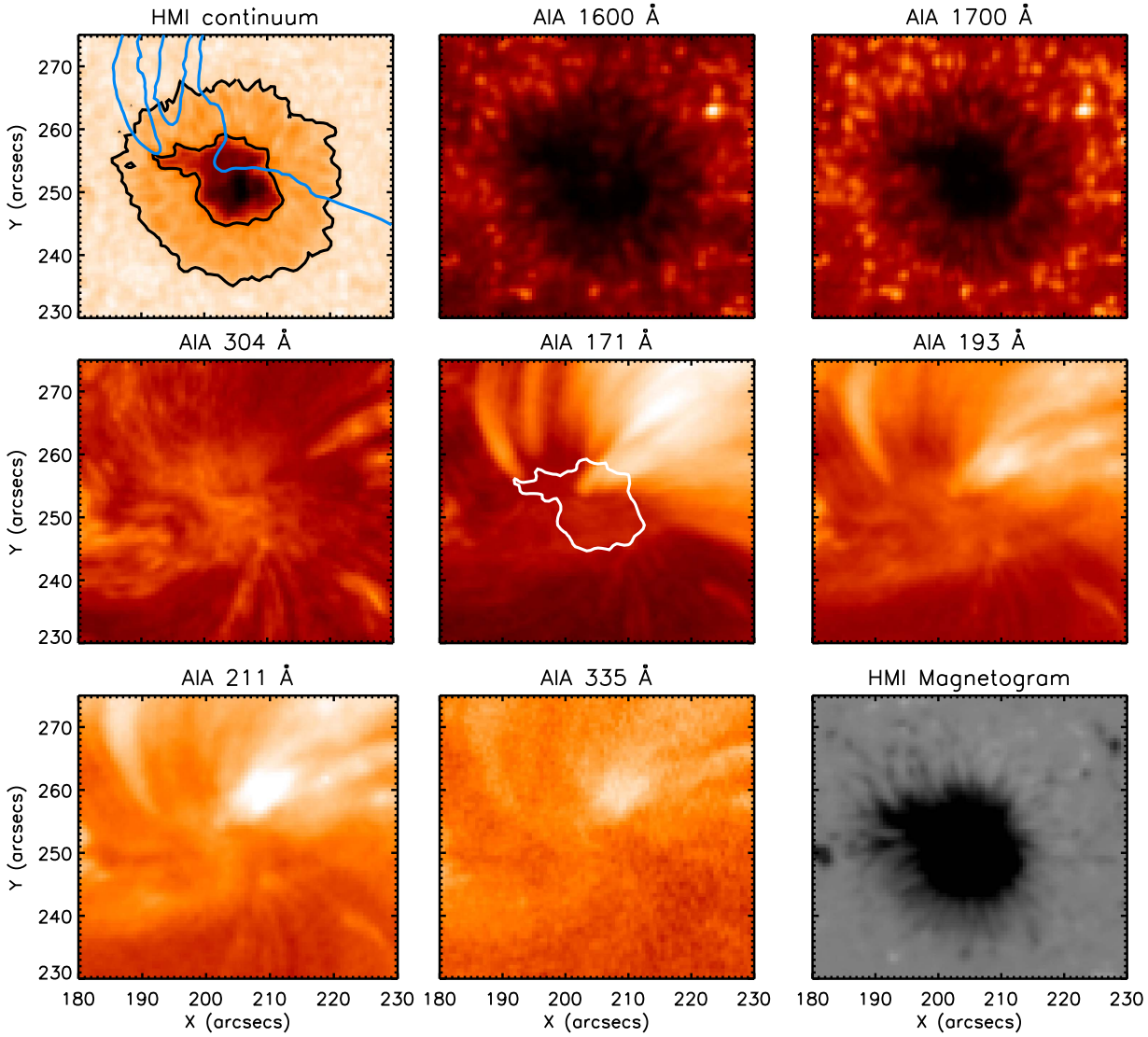

Figure 1. The analyzed sunspot region observed in different AIA and HMI filters. The inner black contour on the top of the HMI continuum image shows the boundary between the umbra and penumbra, whereas the outer one shows the penumbra outer boundary obtained from the HMI continuum. The umbra–penumbra boundary is also shown by a white contour in AIA 171 Å for reference. The overplotted blue contours on the HMI continuum show the locations of fanloops observed in the AIA 171 Å passband.

compared the period of amplitude modulation on Fourier-filtered light curves obtained in different atmospheric layers above the sunspot and associated the presence of slow magnetoacoustic waves in coronal loops with the photospheric p-mode. Zhao et al. (2016) traced p-mode waves from the photosphere to the corona in active regions (ARs) using a time–distance helioseismology analysis technique. However, direct observation of any connection or influence among different sunspot waves and oscillations at different atmospheric layers is still missing.

For direct and unambiguous detection, it is mandatory to have excellent wave signals at different atmospheric layers, which is not always the case. Here, we present an observation where sunspot oscillations were strong enough to show the influence of the perturbation caused by one of the waves on the other waves. Previous such analyses have utilized light curves at individual locations at different atmospheric heights and performed cospatial analysis. However, here we present multi-wavelength analyses on various locations obtained from the time–distance plots. It has helped us to establish a connection between waves in different layers of the solar atmosphere using observations recorded by the Atmospheric Imaging Assembly (AIA, Lemen et al. 2012) on board the *Solar Dynamics Observatory* (*SDO*, Pesnell et al. 2012). We show that umbral flashes influence the propagation of umbral and coronal waves and investigate the characteristics of the different waves with respect to each other. We present the details of the observations in Section 2, data analysis and results in Section 3, and finally summarize our results and conclude in Section 4.

2. Observations

We have analyzed the multi-wavelength observations of AR NOAA *AR 11133* observed by *SDO* on 2010 December 11 between 09:30:00 to 10:15:00 UT. We have used AIA/*SDO* observations in two of its UV channels (1700 Å and 1600 Å) and all of its EUV channels (304 Å, 131 Å, 171 Å, 193 Å, 211 Å, 335 Å, and 94 Å). The data sets for UV have a cadence of 24 s, while those of the EUV channels have a cadence of 12 s. We have also used data from the Helioseismic and Magnetic Imager (HMI) on board *SDO* to provide context. The

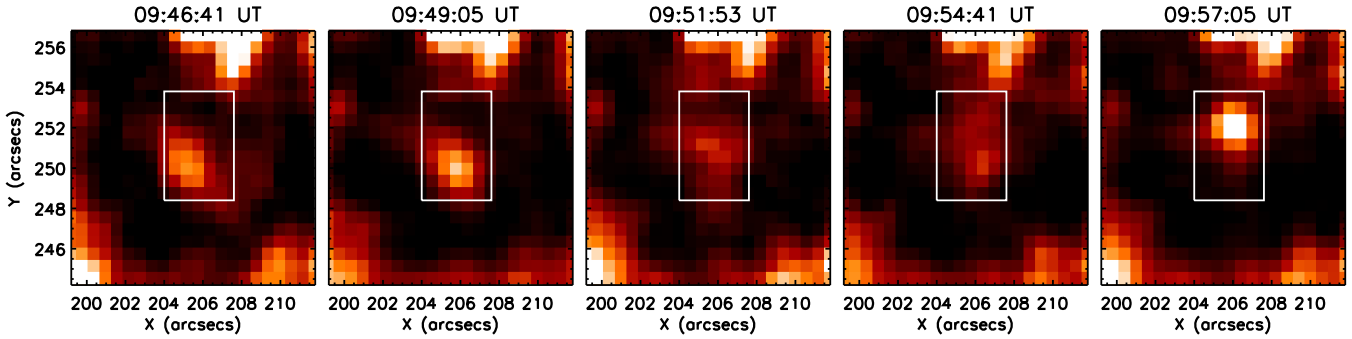

Figure 2. Five umbral flashes observed in AR 11133 in the AIA 1600 Å passband. The white boxes indicate the region within which the flashes occurred.

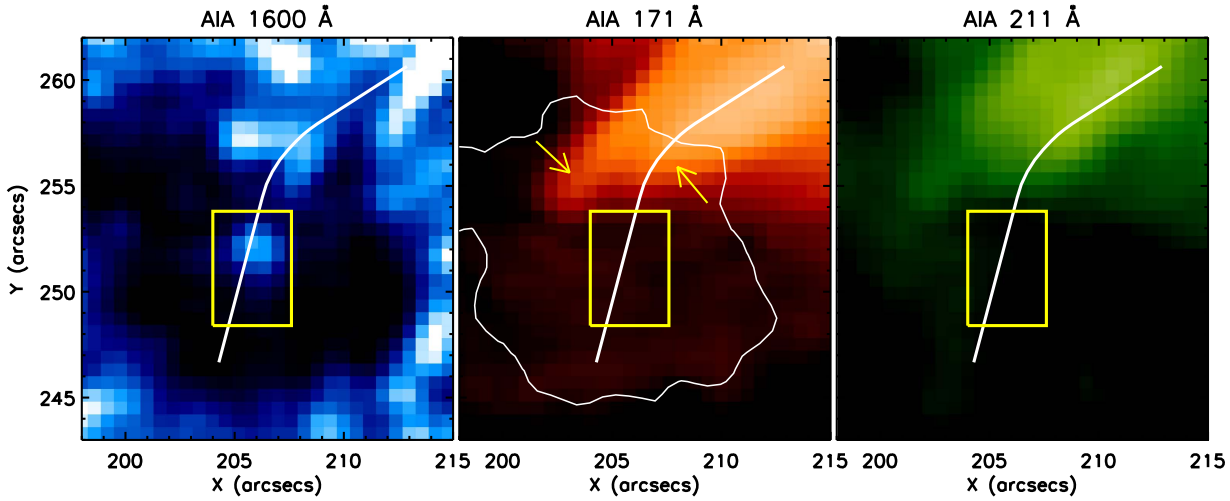

Figure 3. Location of the artificial slit drawn on the top of AIA 1600 Å (left panel), 171 Å (middle panel), and 211 Å (right panel) images along which a time–distance analysis is performed. The yellow boxes on the images show the location of the flashes observed in the AIA 1600 Å passband (shown in Figure 2). The white contour on the top of AIA 171 Å marks the location of the approximate umbra–penumbra boundary obtained from the HMI continuum. The overplotted yellow arrows are directed to the two fanloop systems rooted inside the sunspot umbra.

cadence of the HMI data is 45 s. The spatial resolutions of both the AIA and HMI images are 0.″6 per pixel. The AIA and HMI observations are processed using standard processing software provided in the solar software (SSW) distribution. All the images are co-aligned and derotated with respect to the AIA 171 Å image taken at 9:30:00 UT.

3. Data Analysis and Results

The observed AR mainly consists of a sunspot with fanloops emanating from its upper half. Figure 1 displays the AR in different AIA and HMI passbands. The top left panel shows the analyzed AR in an HMI continuum. The black contours obtained from the HMI continuum show the approximate locations of umbra–penumbra (inner contour) and penumbra outer (outer contour) boundaries. The overplotted blue contours show the fanloop configuration as observed in the AIA 171 Å passband.

3.1. Umbral Flashes, Umbral Waves, and Coronal Waves

We spotted five bright umbral flashes between 09:46:41 UT and 09:57:05 UT in the AIA 1700 Å and 1600 Å passbands, as shown in Figure 2. The overplotted white box encloses the region within which the different umbral flashes occur. In Figure 3, we show the location of umbral flashes on AIA 1600 Å, 171 Å, and 211 Å images. We overplot the approximate umbra-penumbra boundary (white contour) obtained from the HMI continuum on the top of the AIA 171 Å image (middle panel of Figure 3). We find that there are two fanloop systems with coronal footpoints located at different locations of the sunspot umbra (as marked by yellow arrows in Figure 3). To study the effect of perturbation caused by umbral flashes on the surrounding sunspot waves, we adopt a time–distance analysis technique. We show the location of the artificial slit to be used for the time–distance technique in Figure 3. We choose the artificial slit in such a way that it passes through the umbral flashes and also traces a fanloop to observe any influence of flashes on the fanloop. In Figure 4, we show the time–distance maps obtained along this slit in different AIA passbands covering the chromosphere and corona above the sunspot. Maps were obtained by subtracting the background trend of ≈8 minutes running average from each spatial pixel along the time. We tried several ranges of running average windows, and found that 8-minute running averages represent the background/trend signal very well. The time–distance maps clearly show the presence of propagating disturbances in the different layers of the sunspot atmosphere. Five umbral flashes at chromospheric height can be seen in the upper panels of AIA 1600 Å and 1700 Å. The white arrow in the AIA 1700 Å panel indicates the umbral flashes. In the top panels of Figure 4, the yellow dashed lines pass through the approximate location of the umbral flashes, whereas the white

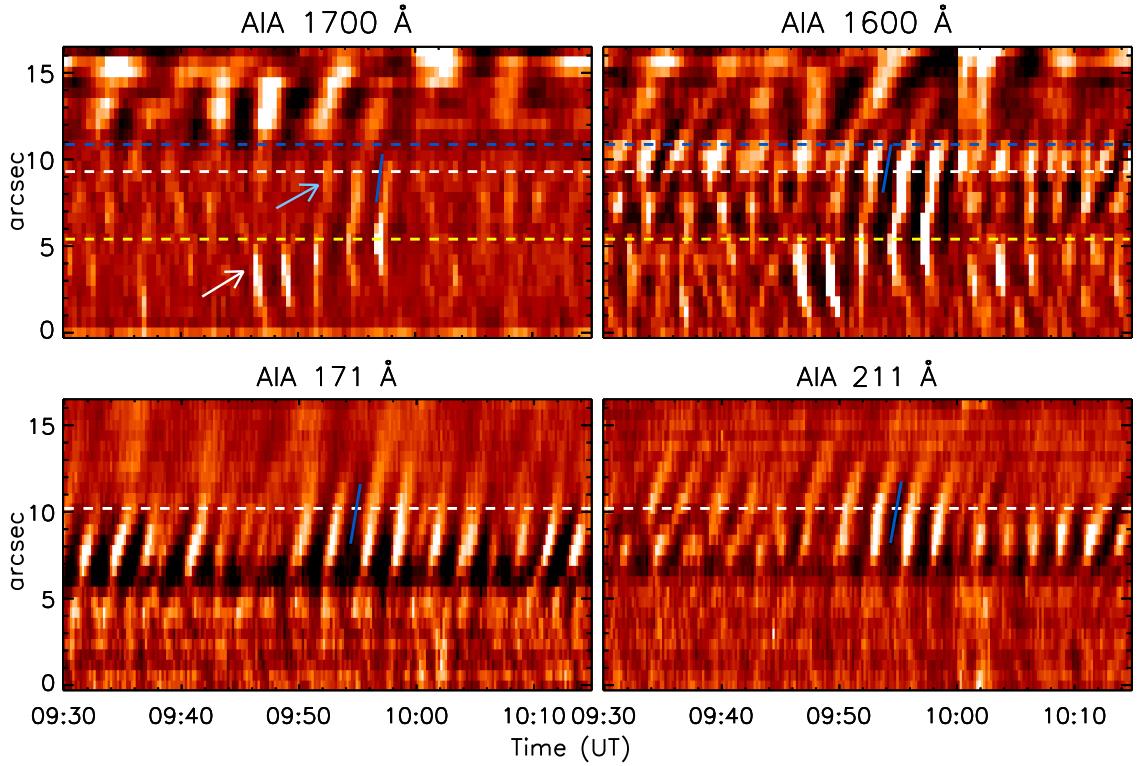

Figure 4. Time–distance plots obtained from different AIA passbands along the artificial slit location shown in Figure 3. In the top left panel, the white arrow points to umbral flashes and the blue arrow points to umbral waves. The dashed yellow horizontal lines indicate the location of umbral flashes. The white horizontal lines on each panel show the locations of the light curves obtained for further analysis. The blue horizontal lines indicate the umbra–penumbra boundary identified from the HMI continuum. The slanted blue lines along the propagating features in each panel are used to measure the average wave propagation speed.

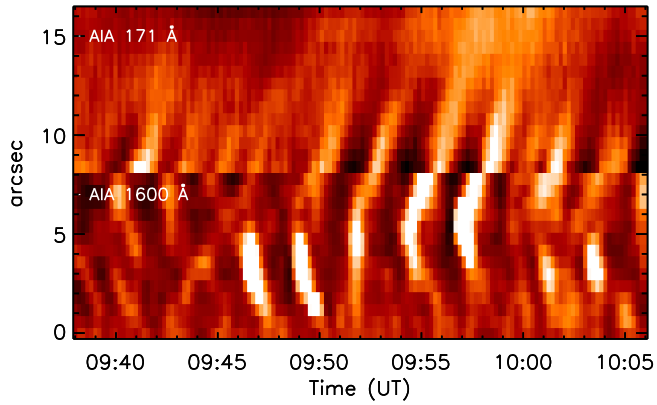

Figure 5. Combined time–distance plot obtained from the AIA 1600 Å and 171 Å passbands for the artificial slit location shown in Figure 3. AIA 1600 Å is plotted from 0″ to 8″, whereas AIA 171 Å is plotted from 8″ to 16″. Intensities are normalized by time-averaged variation along the slit length.

dashed lines pass through the umbral waves. The blue dashed lines show the umbra–penumbra boundary. The time–distance maps clearly reveal the presence of umbral waves emanating from the location of umbral flashes and moving radially outward. The umbral waves are found to be confined to the region between the location of umbral flashes and the umbra–penumbra boundary, i.e., the region between the blue and yellow dashed lines in Figure 4. The blue arrow in the AIA 1700 Å panel shows the propagation of umbral waves originating from the location of umbral flashes. We drew several lines on these propagating features and obtained the average slope and standard deviation that provided the wave propagation speed and associated errors. The umbral wave speeds are found to be quite similar (within errors) in different passbands, with around 66.1 ± 8.7 km s^{-1} for the 1700 Å, 49.0 ± 7.1 km s^{-1} for the 1600 Å, and 56.7 ± 5.1 km s^{-1} for the 304 Å passbands.

Propagating coronal waves are omnipresent along the fanloop in all the AIA coronal passbands for the observed time duration, except in 94 Å, where the signal is too poor to make any conclusive statement. Coronal waves are also detectable for the other fanloops of umbral and penumbral origin (i.e., coronal footpoints cospatial to the umbra and penumbra of the sunspot) as visible in the coronal images of Figure 1. In the bottom panels of Figure 4, we show the presence of coronal waves for the AIA 171 and AIA 211 Å passbands propagating along the analyzed fanloop rooted in the umbra. The white dashed lines in the bottom panels of Figure 4 pass through the coronal waves. The coronal wave speeds are found to be around 50.9 ± 4.9 km s^{-1} for the 171 Å, 46.2 ± 5.3 km s^{-1} for the 193 Å, 46.9 ± 3.6 km s^{-1} for the 211 Å, 62.4 ± 9.2 km s^{-1} for the 335 Å, and 44.8 ± 6.2 km s^{-1} for the 131 Å passbands.

The time–distance maps reveal a peculiar noticeable characteristic for the different sunspot waves. We find an enhancement in the amplitude of the umbral and the coronal waves for the duration of occurrence of the five bright umbral flashes. Enhancements in the amplitudes of coronal waves, which resulted in the triggering of coronal jets, were also observed by Chandra et al. (2015). In order to have a clear picture of the simultaneous amplitude enhancement between different sunspot oscillation and wave modes, we show a combined time–distance map of the chromospheric AIA 1600 Å and coronal AIA 171 Å passbands in Figure 5. The

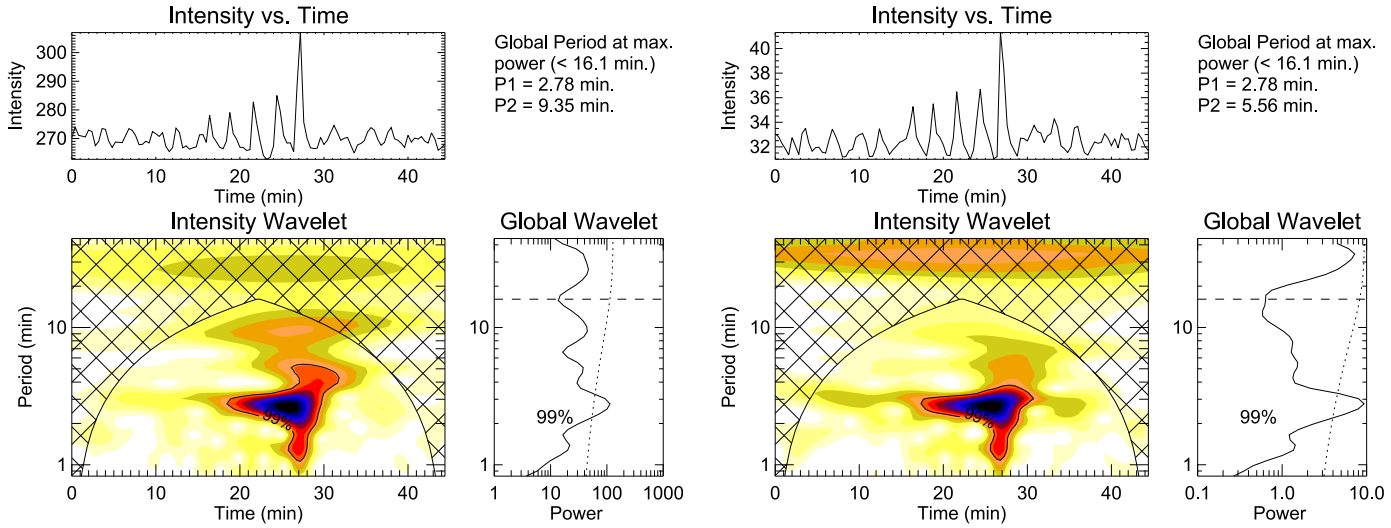

Figure 6. Wavelet analysis results for the light curves obtained at the umbral flash locations (shown in Figure 4) observed in the AIA 1700 Å (left panels) and AIA 1600 Å (right panels) passbands. In each set, the top panels show the variation of the measured intensity with time, where time starts around 9:30 UT. The bottom left panels show the computed wavelet power spectrum (the blue shaded regions represents high power density), while the bottom right panels show the global wavelet power spectrum. The dashed lines in the global wavelet plots indicate the maximum period detectable from wavelet analysis due to the cone-of-influence, whereas the dotted line indicates the 99% confidence level curve. Periods P1 and P2 of the first two power peaks are also printed at the top right.

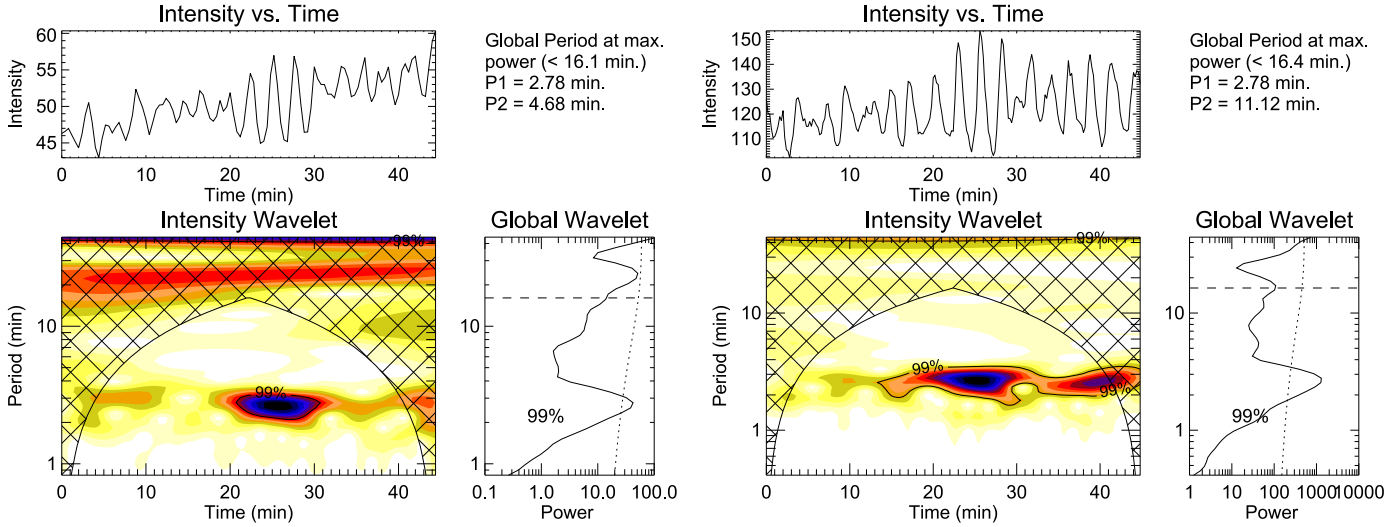

Figure 7. Same as Figure 6, but for umbral waves observed in AIA 1600 Å (left panels) and AIA 304 Å (right panels).

cadence of the AIA 1600 Å images is 24 s, whereas that of the AIA 171 Å images is 12 s. Therefore, we interpolated the AIA 1600 Å images to 12 s cadence to create the combined time–distance map. In this map, we plot AIA 1600 Å from 0″ to 8″ and AIA 171 Å from 8″ to 16″. The resulting map clearly shows an amplitude increase in coronal waves associated with the occurrence of umbral flashes, and thus with umbral waves. The time delay between the two is about 36 s (3-time frames of AIA 171 Å). This indicates that umbral flashes influence the propagation of coronal waves, providing us with the first direct evidence of an influence of umbral flashes on the coronal plasma. We also analyzed the propagation of coronal waves in other fanloops of umbral and penumbral origin, rooted in the same sunspot. In this case, we did not find any influence of umbral flashes in terms of amplitude enhancement in coronal waves propagating along the fanloops of penumbral origin. However, the coronal waves of the other fanloop system rooted in the umbra (left loop in Figure 3) did show some influence of umbral flashes.

The time–distance maps obtained along the artificial slit suggest growth in the amplitude of the waves during 09:44 to 10:00 UT. To analyze this in detail, we obtain light curves at the locations of the umbral flash (yellow dashed line in Figure 4) and the umbral and coronal waves (white dashed lines in Figure 4). We choose the locations on the basis of signal strength. The umbral flash location is averaged over 3″, while the umbral and coronal wave locations are averaged over 1.″2 and 1.″8, respectively. The detailed analyses performed on these light curves are described in the following subsections.

3.2. Wavelet Analysis

We obtain the temporal intensity variations of the umbral flash region, umbral waves, and coronal waves for locations marked in Figure 4. The time evolution of the

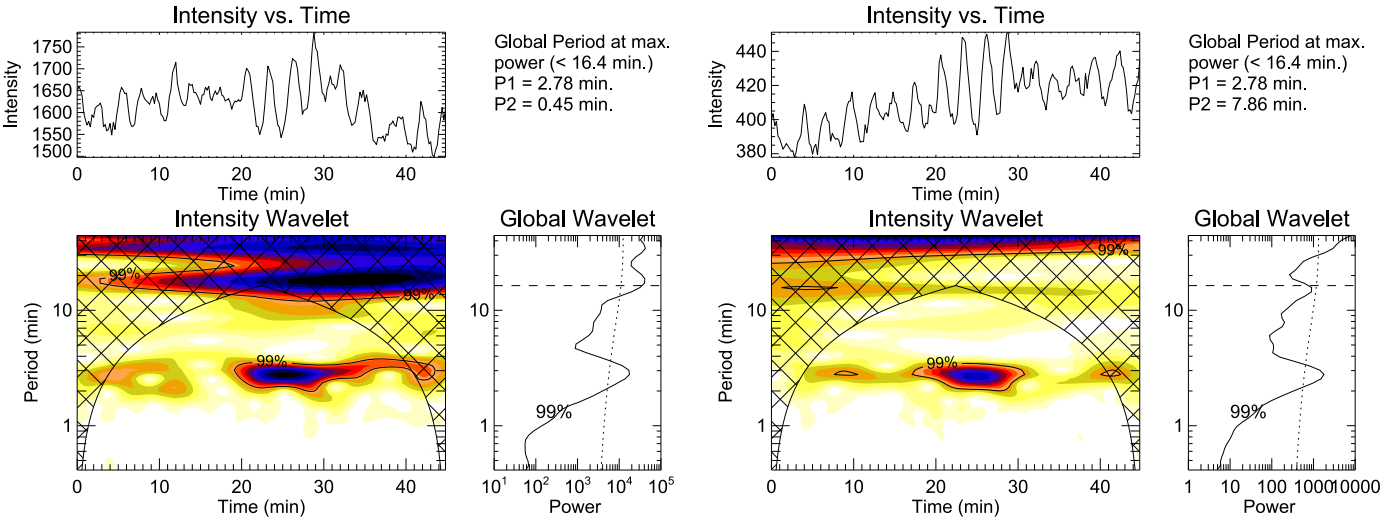

Figure 8. Same as Figure 6, but for coronal waves observed in AIA 171 Å (left panels) and AIA 211 Å (right panels).

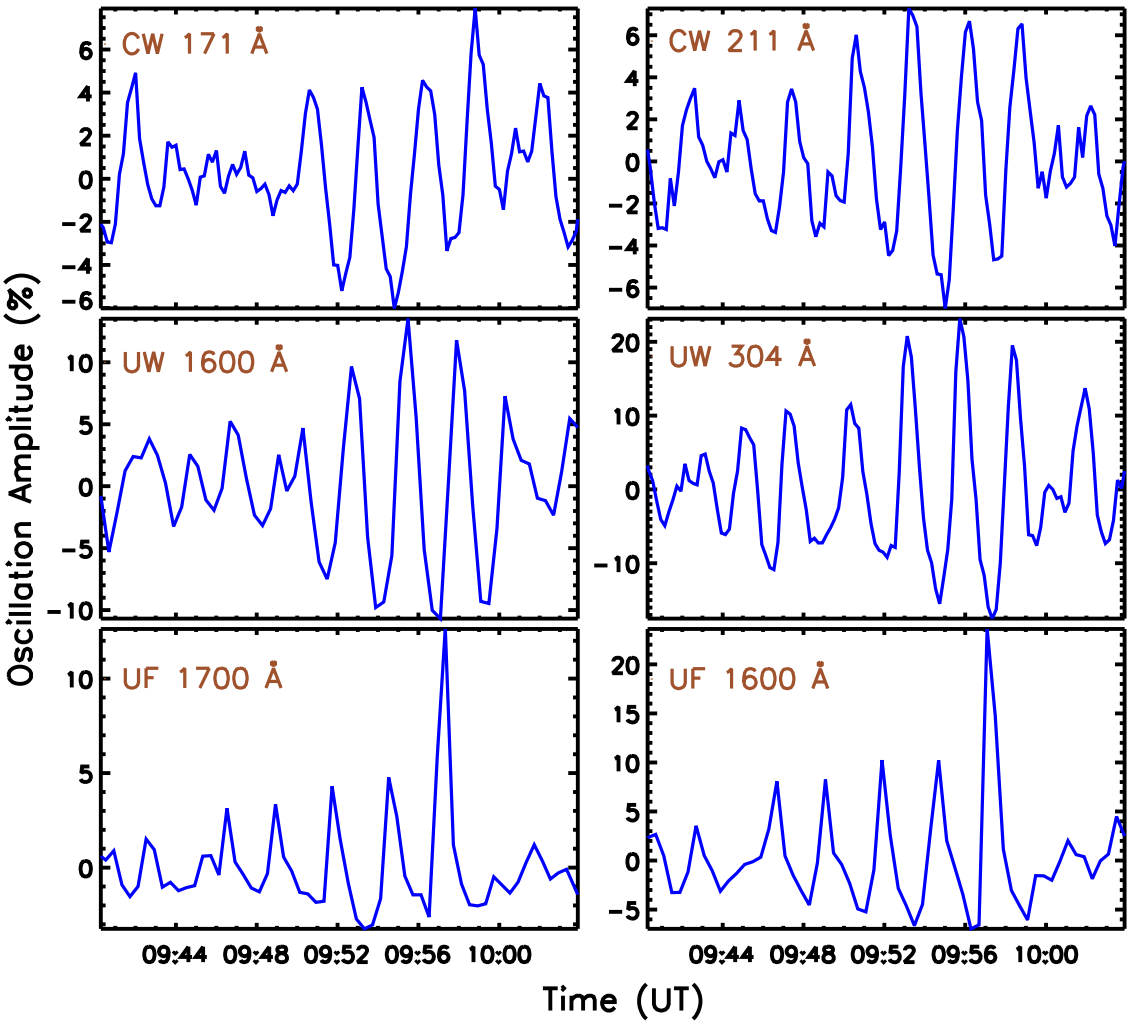

Figure 9. Growing amplitude of different types of sunspot waves and oscillations observed at different layers of the solar atmosphere. The respective locations of the light curves used to obtain the oscillation amplitudes are marked in Figure 4.

intensities obtained from various AIA passbands for different sunspot waves are plotted in the top panels of Figures 6–8. All these intensity light curves show prominent growth in the amplitude of oscillations at similar times as the occurrence of umbral flashes. In all figures, time runs from 9:30 UT to 10:15 UT.

To obtain the periods of these oscillations, we performed wavelet analysis (Torrence & Compo 1998) on all the light

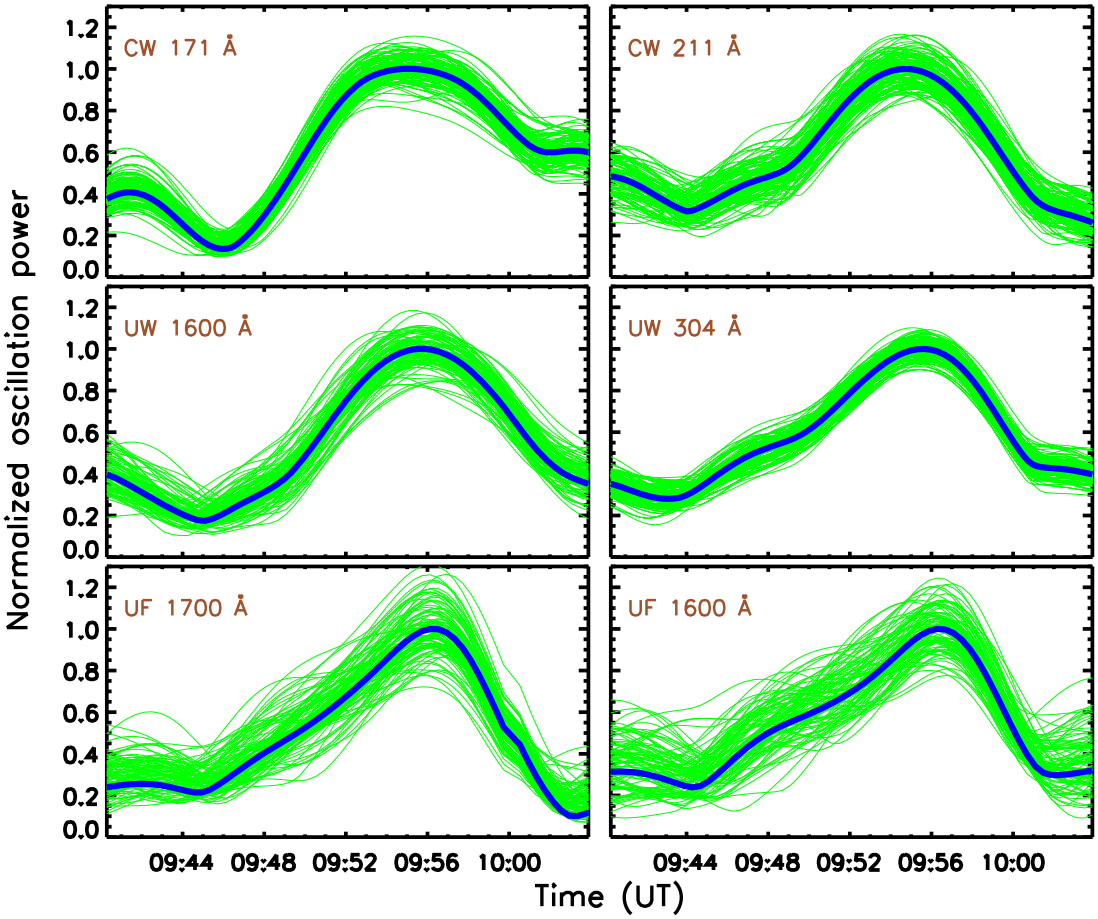

Figure 10. Temporal variation of oscillating power in the period range 2.3–3.3 minutes, obtained from a wavelet transform of different sunspot waves and oscillations. The green curves are obtained by carrying out a wavelet analysis on Monte Carlo bootstrapped light curves. The locations of the analyses are marked in Figure 4.

curves. Wavelet transform provides information on the temporal variation of the frequency of a signal. For this purpose, we chose the Morlet wavelet that is a plane wave with its amplitude modulated by a Gaussian function to convolve with the time series. In Figures 6–8, we show the wavelet results for umbral flashes, umbral waves, and coronal waves, respectively, in different AIA passbands as mentioned in the captions. In each wavelet spectrum (lower left panels), the cross-hatched regions denote the so called cone-of-influence (COI) locations where estimates of oscillation periods become unreliable. This COI is result of edge effects that arise due to the finite lengths of the time series. The global wavelet power, obtained by taking the average over the time domain of the wavelet transform, is also shown for all the sets in the lower right panels. Due to the COI, the maximum period that can be detected from the wavelet transform is shown by a horizontal dashed line in the global wavelet plots of Figures 6–8. The 99% confidence levelis shown in global wavelet plots that are obtained after considering the white noise in the data. We also obtained the first two power peaks from the global wavelet, which are printed in the top right corners of the wavelet plots. The global wavelet plots for umbral and coronal waves show very similar power distributions near the peak period of ≈2.8 minutes. The wavelet analysis results reveal the clear presence of ≈2.8-minute period oscillations for all three sunspot oscillations and waves over the whole observed duration. However, we also noticed that the wavelet powers for this period are not constant and change with time. In the time range between ≈15–30 minutes, wavelet power increases with time for all three sunspot oscillations and waves, and later decreases. This almost cotemporal increase in wavelet power with time in different waves is suggestive of coupling among them, which was also visualized from the time–distance maps in Figure 4.

We further refine our findings by obtaining the oscillation amplitudes of different wave types shown in the top panels of Figures 6–8 and plotted in Figure 9. Oscillation amplitudes are obtained with respect to the background signals, which were obtained from 8-minute running averages of the original light curves, as previously noted. Figure 9 clearly reveals a similar pattern of growth in all the oscillation amplitudes. The amplitude of the oscillations grew by more than 20% for umbral flashes observed in AIA 1600 Å, whereas those for the umbral and coronal waves grew up to ≈10% and 5%, respectively. We also see a sawtooth pattern where the amplitude first increases sharply, and later decreases slowly for umbral flash oscillations. This pattern is also visible in umbral and coronal wave amplitudes, but to a lesser extent. The appearance of the sawtooth pattern may indicate the propagation of shock waves, as suggested by Tian et al. (2014), in the transition region lines. The similarity in the growing amplitudes of oscillation, and the almost cotemporal appearances of umbral flashes with the umbral and coronal waves, are strong indications that these waves are influenced by umbral flashes.

To quantify the amplitude growth of these 2.8-minute oscillations, we look at the oscillatory power of these waves

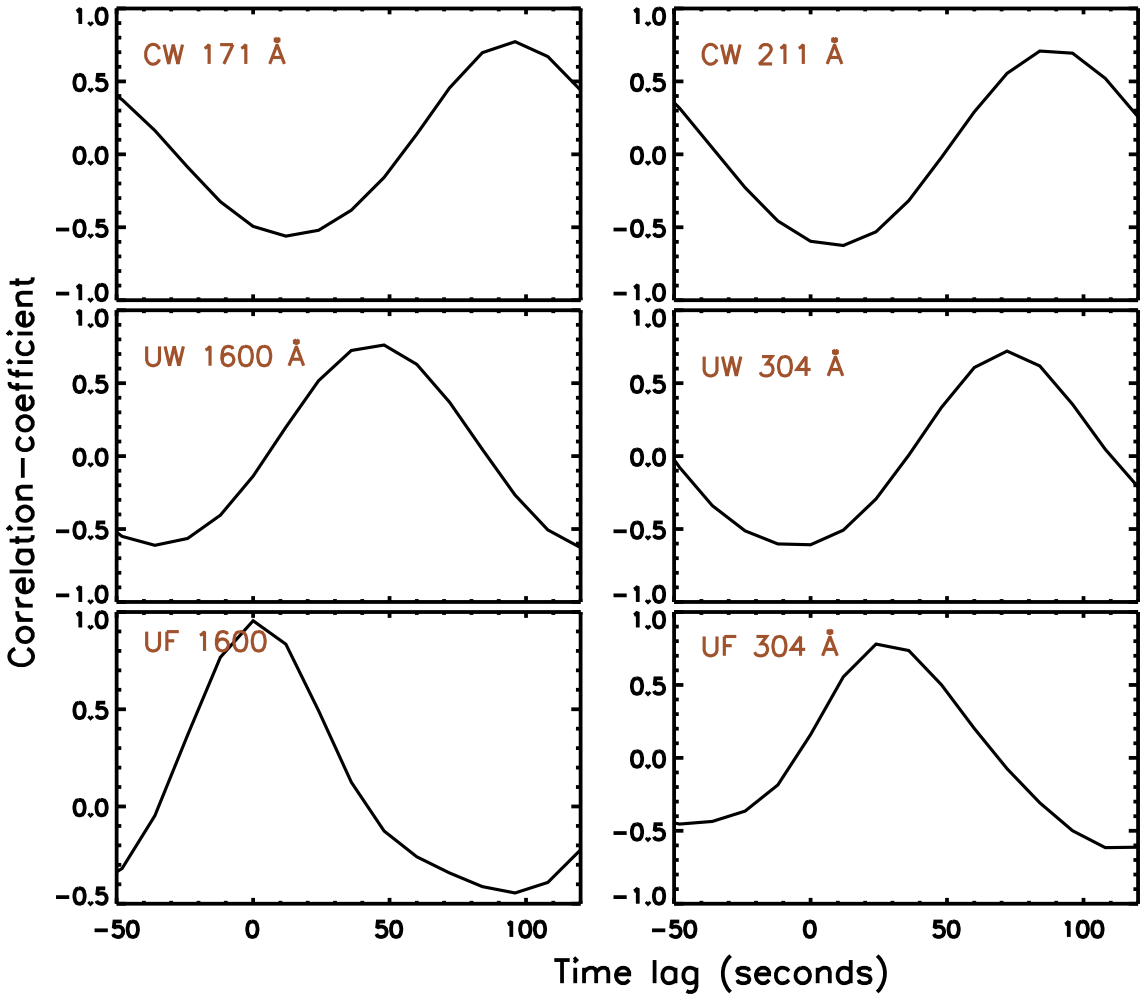

Figure 11. Results of cross-correlation analysis performed on the light curves of different sunspot waves and oscillations with respect to the light curve of the umbral flash location observed from AIA 1700 Å. Cross-correlation coefficients are plotted for different time lags. The locations of the light curves are shown in Figure 4. The types of sunspot waves and oscillations considered for cross-correlation and corresponding passbands are labeled in the respective panels.

with time. Since the wavelet transform provides a temporally variable oscillatory power, we obtain the oscillatory power of these waves with time using the wavelet transforms shown in Figures 6–8. Henceforth, we obtained the wavelet oscillatory power at around a 2.8-minute period averaged over the range of 2.3–3.3 minutes. In Figure 10, we show the oscillatory wavelet power for different oscillations and waves. The upper two panels are shown for coronal waves in AIA 171 and 211 Å, the middle panels are for umbral waves in AIA 1600 and 304 Å, and the bottom panels are for umbral flashes in AIA 1600 and 1700 Å. In each panel, we overplot green curves to show the errors associated with these oscillatory power curves. These error bars are obtained by carrying out the same wavelet analysis on Monte Carlo bootstrapped light curves. In this method, we generate new light curves from the observed one, including point-wise error estimates on the intensities. These are obtained by adding the normalized random distribution of errors to the original light curves. For this purpose, we generated 100 such new light curves. Then, we performed the same wavelet analysis to get a measure of the fuzziness in the results due to statistical fluctuations. The respective error bars on the AIA light curves were obtained using the routine *aia_bp_estimate_error* (Boerner et al. 2012). The plots show almost similar power characteristics for all the waves. Given the range of error bars, we conclude that the consistent growth observed in wavelet powers (in the period range 2.3–3.3 minutes) between 09:44:00 and 10:00:00 UT is real. Thus, finding an almost cotemporal increase of oscillatory power in around 2.8-minute periods further strengthens our claim of association between umbral flashes and waves, and coronal waves.

3.3. Time-delay Analysis

To further strengthen and understand the probable coupling among different waves and oscillations, we performed a cross-correlation analysis of these waves for the duration 09:43:00 UT to 10:00:00 UT. The time is chosen such that it covers the time of occurrence of the umbral flashes. This enables us to observe the time lags associated with the maximum correlation coefficients, and hence to determine the time delays between different waves. We choose the light curve of umbral flashes obtained using 1700 Å images to perform the cross-correlation with light curves of umbral flashes observed in 1600 and 304 Å, umbral waves observed in 1600, and 304 Å, and coronal waves observed in 171 and 211 Å.

Figure 11 displays the results of a cross-correlation analysis in terms of the correlation coefficients obtained for different time

lags. The analysis is performed using the standard IDL routine *c_correlate*, which finds the correlations among the amplitudes of oscillations of different sunspot waves and oscillations. The plots reveal around a 70% correlation for all the waves with respect to the AIA 1700 Å umbral flash oscillations. We observe an increase in time delay corresponding to the peak correlation coefficient as we go from chromospheric umbral flashes and umbral waves to coronal waves. The time delay increases because the distance at which light curves were obtained increases for umbral waves and coronal waves with respect to umbral flash location (see Figure 4). However, time delays obtained from the AIA 304 Å passband are relatively larger for umbral flash and waves, as compared to the AIA 1600 Å passband. This may indicate that AIA 304 Å forms at a higher atmospheric height compared to the AIA 1700 and 1600 Å passbands. Furthermore, we do not find any significant time delays among the coronal passbands. This could be attributed to the fact that emissions in different AIA passbands are coming from the lower-temperature components, as fanloops are typically of 1 MK temperature (e.g., Ghosh et al. 2017). The significantly correlated light curves observed in chromospheric umbral flashes with umbral waves and coronal waves confirm the influence of umbral flashes on umbral waves and coronal waves.

4. Summary and Conclusions

In this paper, we have focused on different types of sunspot oscillations and waves observed at solar chromospheric and coronal heights. We explored the sunspot with the AIA 1700 Å, 1600 Å and 304 Å passbands and the fanloop region over it with AIA 131 Å, 171 Å, 193 Å, 211 Å, and 335 Å passbands. We list our findings below.

1. Five bright umbral flashes were identified from the AIA 1700 Å, 1600 Å, and 304 Å images (shown in Figures 2, and 3). Their locations were found in close proximity to the footpoint of one of the fanloops that was rooted in the umbra (shown in Figure 3).
2. The emergence of umbral waves moving radially outward was observed in the AIA 304 Å, 1600 Å, and 1700 Å passbands from the locations of umbral flashes (shown in Figure 4). The amplitude of umbral waves increased during the umbral flashes.
3. Almost all the AIA coronal passbands showed signatures of propagating magnetoacoustic waves along the different fanloop structures, with umbral and penumbral origins. However, the fanloop systems that were rooted inside the sunspot umbra showed oscillations with modulations in amplitude (shown in Figure 4). A combined time–distance plot of chromospheric AIA 1600 Å and coronal AIA 171 Å showed a simultaneous amplitude increase in coronal waves that could be associated with the umbral flashes, and thus, with umbral waves (shown in Figure 5). Hence, the increasing amplitude of the coronal waves could be influenced by the occurrence of umbral flashes. Moreover, the umbral flash light curves, and sometimes (to a lesser extent) umbral waves and coronal waves light curves reveal a clear sawtooth pattern of oscillations (shown in Figure 9), which can be attributed to a chromospheric response to the magnetoacoustic shock due to propagating photospheric p-mode oscillations (e.g., Centeno et al. 2006; Tian et al. 2014).
4. Using wavelet analysis, we obtained periods of oscillation of the different sunspot waves. For all the waves, i.e., umbral flash, umbral waves, and coronal waves, the dominant period was ≈2.8 minutes (shown in Figures 6–8). The cotemporal growth of 2.8-minute oscillations for all the sunspot waves and oscillations was also suggested by the temporal variation of wavelet power (shown in Figure 10, which shows simultaneous growth in wavelet power for all the sunspot waves and oscillations).
5. The significant correlations among chromospheric umbral flash, umbral waves, and coronal waves with some time delays is an indication of propagations of sunspot oscillations and waves from the lower atmosphere to the upper atmosphere (shown in Figure 11).

The results obtained here provide the first direct observational evidence of the influence of chromospheric umbral flashes on umbral waves and coronal waves. These results are supported by the time–distance maps and simultaneous growth in oscillation amplitudes obtained from the original light curves. Though our results are based on the analysis of original, unfiltered light curves, we also performed the same analysis using the Fourier-filtered light curves obtained within the frequency range 5–7 mHz (≈2.3–3.3 minutes). The Fourier-filtered light curves also yielded a similar cotemporal pattern for different sunspot oscillations and waves in the different AIA passbands. Our results point toward the occurrence of a few strong umbral flashes that influence the propagation of all the sunspot waves and oscillations observed at different solar atmospheric layers. Hence, we show the effect of chromospheric umbral flashes in the corona. The analysis presented here also provides important findings for understanding the trigger mechanism of coronal jets. Chandra et al. (2015) suggested that jets were triggered due to an increase in the amplitudes of waves. This analysis provides a reason for the increase and therefore important results for the initiations of jets.

To further confirm and establish these findings, coordinated observations of sunspots waves and oscillations using simultaneous ground- and space-based facilities are essential. The Solar Ultraviolet Imaging Telescope (SUIT; Ghosh et al. 2016) on board Aditya-L1 will provide excellent coverage of the photosphere and chromosphere to study the coupling of these waves in more detail.

A.S. thanks IUCAA for providing local hospitality and support during her stay. G.R.G. is supported through the INSPIRE Faculty Award of the Department of Science and Technology (DST), India. D.T. acknowledges the support from the Max-Planck Partner Group on Coupling and Dynamics of the Solar Atmosphere at IUCAA. V.K. was supported through NASA Contract NAS8-03060 to the *Chandra* X-ray Center. Part of this work was done during collaborative visits that were part of the ClassACT—an Indo-US Centre for Astronomical Object and Feature Characterization and Classification, sponsored by the Indo-US Science and Technology Forum (IUSSTF). A.P. acknowledges a visiting associateship of IUCAA. The authors thank Drs. Dipankar banerjee, David Jess, and Krishna Prasad for helpful discussions. AIA and HMI data are courtesy of *SDO* (NASA).

Facilities: SDO (AIA, HMI).

ORCID iDs

G. R. Gupta https://orcid.org/0000-0002-0437-6107
Durgesh Tripathi https://orcid.org/0000-0003-1689-6254
Amit Pathak https://orcid.org/0000-0001-6328-4512

References

Beckers, J. M., & Tallant, P. E. 1969, SoPh, 7, 351
Bloomfield, D. S., Lagg, A., & Solanki, S. K. 2007, ApJ, 671, 1005
Boerner, P., Edwards, C., Lemen, J., et al. 2012, SoPh, 275, 41
Bogdan, T. J., & Judge, P. G. 2006, RSPTA, 364, 313
Centeno, R., Collados, M., & Trujillo Bueno, J. 2006, ApJ, 640, 1153
Chandra, R., Gupta, G. R., Mulay, S., & Tripathi, D. 2015, MNRAS, 446, 3741
Christopoulou, E. B., Georgakilas, A. A., & Koutchmy, S. 2000, A&A, 354, 305
Christopoulou, E. B., Georgakilas, A. A., & Koutchmy, S. 2001, A&A, 375, 617
De Moortel, I. 2009, SSRv, 149, 65
De Moortel, I., Ireland, J., Hood, A. W., & Walsh, R. W. 2002, A&A, 387, L13
De Moortel, I., & Nakariakov, V. M. 2012, RSPTA, 370, 3193
Ghosh, A., Chatterjee, S., Khan, A. R., et al. 2016, Proc. SPIE, 9905, 990503
Ghosh, A., Tripathi, D., Gupta, G. R., et al. 2017, ApJ, 835, 244
Gupta, G. R., Banerjee, D., Teriaca, L., Imada, S., & Solanki, S. 2010, ApJ, 718, 11
Gupta, G. R., Teriaca, L., Marsch, E., Solanki, S. K., & Banerjee, D. 2012, A&A, 546, A93
Jess, D. B., De Moortel, I., Mathioudakis, M., et al. 2012, ApJ, 757, 160
Jess, D. B., Reznikova, V. E., Van Doorsselaere, T., Keys, P. H., & Mackay, D. H. 2013, ApJ, 779, 168
Kiddie, G., De Moortel, I., Del Zanna, G., McIntosh, S. W., & Whittaker, I. 2012, SoPh, 279, 427
Kobanov, N. I., Kolobov, D. Y., & Makarchik, D. V. 2006, SoPh, 238, 231
Kobanov, N. I., & Makarchik, D. V. 2004, A&A, 424, 671
Krishna Prasad, S., Banerjee, D., & Gupta, G. R. 2011, A&A, 528, L4
Krishna Prasad, S., Jess, D. B., & Khomenko, E. 2015, ApJL, 812, L15
Lemen, J. R., Title, A. M., Akin, D. J., et al. 2012, SoPh, 275, 17
Madsen, C. A., Tian, H., & DeLuca, E. E. 2015, ApJ, 800, 129
Pesnell, W. D., Thompson, B. J., & Chamberlin, P. C. 2012, SoPh, 275, 3
Rouppe van der Voort, L. H. M., Rutten, R. J., Sütterlin, P., Sloover, P. J., & Krijger, J. M. 2003, A&A, 403, 277
Sych, R. 2016, GMS, 216, 467
Thomas, J. H., & Weiss, N. O. 2008, Sunspots and Starspots (Cambridge: Cambridge Univ. Press)
Tian, H., DeLuca, E., Reeves, K. K., et al. 2014, ApJ, 786, 137
Torrence, C., & Compo, G. P. 1998, BAMS, 79, 61
Tziotziou, K., Tsiropoula, G., Mein, N., & Mein, P. 2006, A&A, 456, 689
Zhao, J., Felipe, T., Chen, R., & Khomenko, E. 2016, ApJL, 830, L17
Zirin, H., & Stein, A. 1972, ApJL, 178, L85